Progress In Electromagnetics Research C, Vol. 106, 1–16, 2020

A Hybrid Multi-Port Antenna System for Cognitive Radio

Rajeev K. Parida[1, *], Rashmirekha K. Mishra[2], Nihar K. Sahoo[1], Arjuna Muduli[3], Dhruba C. Panda[1], and Rabindra K. Mishra[1]

Abstract—This paper proposes a hybrid, compact, low profile, and multi-port antenna system for Cognitive Radio (CR). This system consists of a CPW-fed sensing UWB monopole (2–11 GHz) and three NB antennas, out of which one is standalone (7.355 GHz); one is dual-band (5.834 GHz and 8.786 GHz); and the other is reconfigurable (3.863 GHz, 4.664 GHz, 5.2 GHz, and 6.13 GHz) using switching mechanism. This antenna system exhibits less than −15 dB isolation over the operating band. The system is simulated using CST Microwave Studio, and a prototype is fabricated to verify the results. The simulated results are in good agreement with measured ones. The proposed antenna is suitable to operate in C-band, ISM/WLAN/Military application, mid-band 5G, maritime radio navigation, X-band satellite communication, and public safety wireless communication.

1. INTRODUCTION

Applications of Cognitive Radio (CR) gained momentum after the Federal Communication Commission allowed the 3.1–10.6 GHz band for commercial use [1]. This created opportunities for many non-commercial applications of CR technology, which is based on spectrum sharing when the spectrum is not in use. A case study says that at some place and time up to 80% of the allocated spectrums remain idle, which justifies the usability of this technology [2, 3]. The performance of a CR depends on its antenna system [4]. A CR antenna system needs a compact, low profile, UWB antenna for continuous unused spectrum monitoring. If any channel is free, it establishes communication through an integrated narrowband (NB) antenna in that channel. Several designated bands within UWB are classified for communication such as C-band, ISM, WLAN, and Mid-band 5G [5, 6]. To use these bands, there is a requirement of more NB antennas to cover the UWB spectrum. It is a challenging task to pack all these NB antennas and the UWB antenna in the design of such an antenna system in a limited space [7, 8]. In a CR antenna, the UWB antenna occupies most of the space. Several miniaturization techniques have been implemented to reduce the size of UWB monopole antenna [9, 10]. They include the use of a modified ground plane structure which helps in minimizing the cross-polarization level and improving impedance matching. But, it affects antenna gain and radiation patterns [11, 12]. For modeling the CR antenna system, a planar CPW fed UWB antenna is preferred [13], as it offers easy integration of NB communicating antennas within a compact space.

Some notable integrated CR antenna systems include coverage of: 3–11 GHz sensing band and four communicating sub-bands using a dimension of $68 \times 54 \times 0.79\,\text{mm}^3$ [14]; 2–5.5 GHz sensing band and 2.6–2.7 GHz communicating band using a dimension of $80 \times 65 \times 1.58\,\text{mm}^3$ [15]; 3.3–12 GHz sensing band and two communicating sub-bands using a dimension of $58.35 \times 75.7 \times 0.762\,\text{mm}^3$ [16]. Besides, a multiport antenna system of size $120 \times 65 \times 1.56\,\text{mm}^3$ reported in [17] uses two widebands for spectrum sensing and seven sub-bands for communication purpose. In this antenna system, a large sensing antenna is

Received 27 May 2020, Accepted 15 September 2020, Scheduled 2 October 2020

* Corresponding author: Rajeev Kumar Parida (rkparida91@gmail.com).

[1] Department of Electronic Science and Technology, Berhampur University, Odisha, India. [2] School of Electronics Engineering, KIIT, Bhubaneswar, Odisha, India. [3] Department of ECE, Koneru Lakshmaiah Education Foundation, Greenfield, Vaddeswarm, Andhra Pradesh, India.

used as a ground plane for other NB antennas. A recent review of the CR antenna system is reported in [18]. However, the above discussed integrated CR systems have some drawbacks, like poor gain and efficiency, lower sensing bands, fabrication complexity, large antenna dimension, and low isolation among antennas. Improvement of isolation, without increasing size, needs additional components such as microstrip lines, slots, strips, metamaterials, energy bandgap structure, defected ground planes, complementary split-ring resonators, etc. [22]. Avoiding such additional circuitry to improve isolation is still an open problem. Further, many researchers reported reconfigurable communicating antennas for CR [23–25]. The reconfiguration can be achieved using PIN diodes, varactor diodes, RF-MEMS, FETs, stepper motors, and photoconductive elements [26, 27]. However, these switching techniques have issues like non-linearity effects, low switching speed, additional power requirements, etc. [28]. To overcome these issues, we propose a multiport antenna system and limit the number of diodes used for reconfiguration. Furthermore, efficient utilization of the space in a CR system [29] continues to be an important problem, as inefficient utilization of available system area limits the number of NB states.

This paper focuses on the proper utilization of the available area in a CR system to maximize the number of NB states and isolation among antennas. To this end, the paper proposes a modified CPW-fed monopole to cover the sensing UWB band and reused its ground plane for some communicating NB antennas besides adding a reconfigurable NB antenna limiting the number of p-i-n diodes (for reconfiguration) to three. In total, the proposed CR antenna system uses a UWB antenna, one NB antenna, one dual-band NB antenna, and a reconfigurable NB antenna using a small substrate working in cohesion without interference or significant coupling. For ground plane reuse, this work is different from other reported ones. For example, in reference [28], one ground plane is used for three monopole antennas (one sensing and two NB). This is extended further in [30] with the addition of two more monopole antennas on the opposite side with separate ground planes for each of them. Similarly, in reference [31], the authors used one ground plane with four slots to accommodate monopole antennas. All these come under "use of a common ground plane" instead of "ground plane reuse". In our case, the ground plane is used by the sensing antenna which is a CPW-fed monopole, and reused by communicating microstrip antennas. These antennas belong to two distinct classes of planar antennas, which use one ground plane. So, the term "ground plane reuse" is more appropriate in our case. Moreover, the communicating antennas in reference [28] cover only the upper half of the UWB spectrum using four distinct bands each limited to within 1 GHz bandwidth. Those in reference [30] cover the full band using five bands, three of which have bandwidths above 1 GHz. The antenna system in reference [31] uses three broadband antennas for communication. In the CR system, for high reliability communicating antennas are expected to be narrowband in nature and hence these are termed as narrowband (NB) antennas. To achieve this, suitable antenna can be dual-band, multiband or reconfigurable in nature, covering a major portion of the UWB spectrum. Our proposed antenna meets all these requirements with a maximum bandwidth of NB antennas limited to 1 GHz.

2. ANTENNA DESIGN

Figure 1 shows the proposed antenna structure. The antenna connected to Port-1 is a CPW monopole UWB antenna. To Port-2 and Port-3, respectively, U-slot and G-shaped NB antennas are connected. A reconfigurable NB antenna is connected to Port-4.

2.1. UWB Sensing Antenna

Keeping the ground plane reusability in mind, we considered a CPW-fed circular monopole [32]. When the monopole is other than a circular shape, the first resonating frequency depends on its effective radius. The performance of a CPW-fed monopole primarily depends on its effective radius, feed-gap, and width of the ground plane. It is independent of the length of the ground plane beyond a definite length [32]. The width of the CPW ground affects impedance matching and bandwidth. Initially, we fixed the ground plane size to an acceptable value. We saw that it affected the impedance values. To improve the impedance performance [33], we placed a half-pentagon on the upper portion of the circular monopole, as shown in Fig. 2. This is in agreement with [33] that vertex truncation in the feed portion improves bandwidth (BW) performance. The lower circular portion is like trimming at

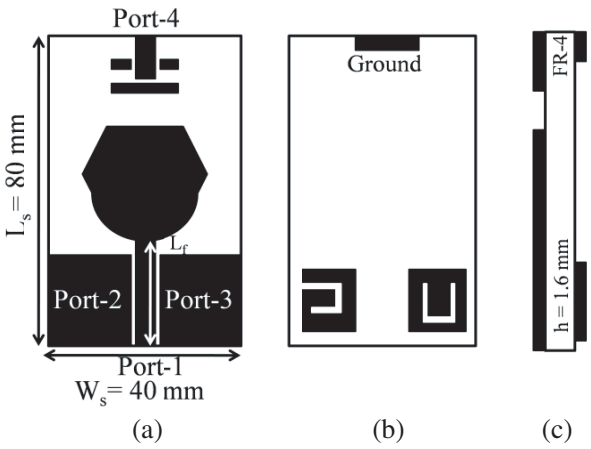

Figure 1. Proposed CR antenna system, (a) front view, (b) bottom view, and (c) side view.

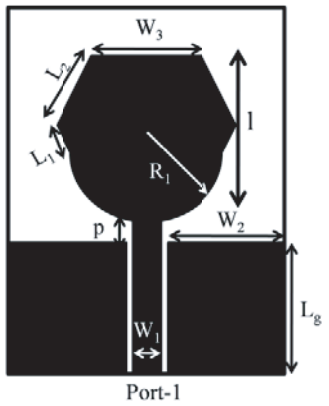

Figure 2. UWB monopole sensing antenna.

multiple points of the vertex. The pentagon part improves the impedance performance due to uniform current distribution, and the lower circular portion improves the bandwidth. It is known that BW of a circular monopole is greater than that of other shapes. In this way, we minimized ground plane size and achieved UWB. The optimal dimensions are obtained by parametric sweep. The ground plane dimension is between 47 mm [32] and 30 mm [35]. A larger ground plane will increase the overall CR antenna size, and a smaller ground may not provide sufficient ground to place NB antennas. Therefore, to obtain an optimal design with acceptable ground plane size, we concentrated more on the radiating patch. Table 1 shows the considered optimal dimensions of the antenna for a lower cut-edge frequency of 2.0 GHz.

The lower cut-edge frequency f_L and corresponding wavelength λ_L of the monopole are defined using Eq. (1).

$$f_L = \frac{c}{\lambda_L} = \frac{7.2}{\{(l + r + p) \times k\}} \text{ GHz} \tag{1}$$

where l, r, and p are the equivalent cylindrical height, radius, and gap between the ground plane and radiating patch of the antenna [34]. The value of k is different for different dielectric materials which is chosen empirically to obtain lower resonant frequency. The initial dimensions are fixed using Eqs. (2)–(7) [34, 35]. The height of the monopole antenna (l) is $\lambda_L/4$ [36].

The equivalent radius of the radiating patch is fixed according to Eqs. (2) and (3).

$$0.0625\lambda_L \leq r \leq 0.125\lambda_L \tag{2}$$

$$r \approx \frac{\lambda_L}{6} - 0.5L_f \tag{3}$$

Table 1. Design parameters of CR antenna.

UWB sensing antenna		**G-shaped NB antenna**		**U-slot NB antenna**		**Reconfigurable NB antenna**	
Parameters	**Size (mm)**	**Parameters**	**Size (mm)**	**Parameters**	**Size (mm)**	**Parameters**	**Size (mm)**
L_1	5.83	L_4	9	L_9	7.50	L_{13}	1.3
$L_2 = W_3$	14.80	L_5	2	L_{10}	7	$L_{14} = W_1$	3
L_g, p	16, 0.5	L_6	6	L_{11}	5	L_{15}	15.5
W_1	3	L_7	3	L_{12}	4.50	W_9	13
W_2	18.20	L_8	5	W_6	3	W_{10}	4.50
R_1	12	W_4, W_5	9.50, 7.50	W_7,W_8	3.50, 0.25	W_{11}	7

The gap between ground plane and radiating patch of the antenna ($p = L_f - L_g$) can be determined using Eq. (4).

$$(L_f - L_g) \leq 0.02\lambda_L \tag{4}$$

The length (L_s), width (W_s), and thickness (h) of the substrate can be determined using Eqs. (5) to (7). The total length of the substrate for the integrated structure containing all elements needs to be $0.5L_g$ more than that of the sensing element alone. This requires that the substrate dimension should conform to the following.

$$0.25\,(\lambda_L + 2L_g) \leq L_S \leq 0.5\,(\lambda_L + L_g) \tag{5}$$

$$W_s \approx 4r \tag{6}$$

$$h \approx 0.01\lambda_L \tag{7}$$

2.2. G-Shaped and U-Slot NB Antenna

A spur-line slot on a rectangular patch antenna creates an extra resonance [37]. We call this antenna as a G-shaped antenna after the spur-line slot is made as shown in Fig. 3. The U-slot antenna is well documented in the literature [38]. The G-shaped antenna is, in fact, another U-slot antenna with one smaller slot arm. The larger slot arm extends to the edge of the patch. The design of the G antenna starts with that for the U-slot antenna and settles down through parametric studies. The insertion direction is chosen such that it does not disturb the current distribution on the CPW feed-line. This avoids coupling with the sensing antenna. Optimal dimensions of the antenna for the desired band obtained using CST Microwave Studio, are shown in Table 1. Fig. 4 shows the U-slot rectangular patch antenna. The U-slot shifts the resonant frequency towards the lower side [39]. It operates in a single band mode. CST Microwave Studio gives the optimal dimension of the antenna after parametric analyzes. Table 1 shows the physical parameters of the antenna.

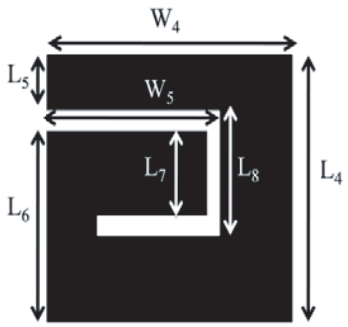

Figure 3. G-shaped NB patch antenna.

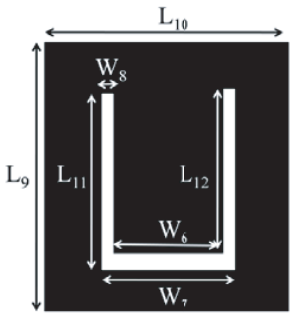

Figure 4. U-slot NB patch antenna.

2.3. Reconfigurable NB Antenna

The reconfigurable planar monopole on a partial ground plane is inspired by [40]. Its geometrical parameters, corresponding to four intended frequency bands, are obtained using parametric studies. It operates in three single and a dual-band mode. The reconfiguration can be achieved using three p-i-n diodes [23–26], for which variable resistors can be its equivalent circuits. The frequency agility functionality of the antenna depends on the switching states of the p-i-n diodes modeled by their equivalent circuits [41]. The proposed reconfigurable antenna is shown in Fig. 5.

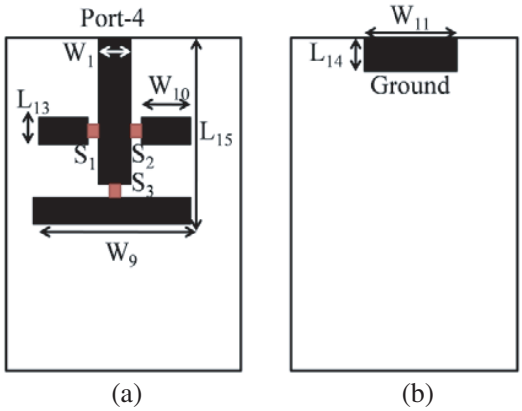

Figure 5. Reconfigurable NB monopole antenna, (a) top view and (b) bottom view.

3. RESULTS AND DISCUSSION

To study the performances of the proposed antenna, CST Microwave Studio is used. Also, we fabricated a prototype on an FR-4 substrate ($\varepsilon_r = 4.4$ and loss tangent $= 0.02$) of dimension $80 \times 40 \times 1.6\,\text{mm}^3$, shown in Fig. 6. Fig. 7 shows the measurement setup, using a VNA, in an anechoic chamber.

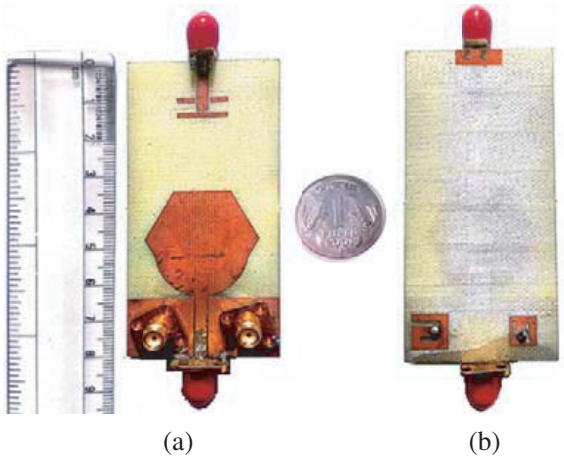

Figure 6. Fabricated antenna prototype, (a) top and (b) bottom view.

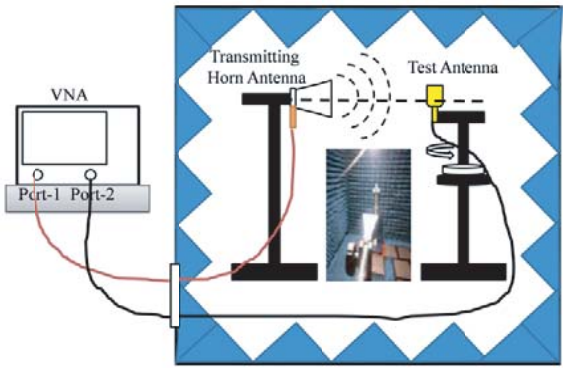

Figure 7. Setup for radiation pattern measurement inside anechoic chamber.

3.1. UWB Sensing Antenna

Figure 8 compares the reflection coefficient (S_{11}) obtained from simulation and measurement over the frequency band of 2 GHz to 11 GHz. Both plots follow each other in close proximity, indicating

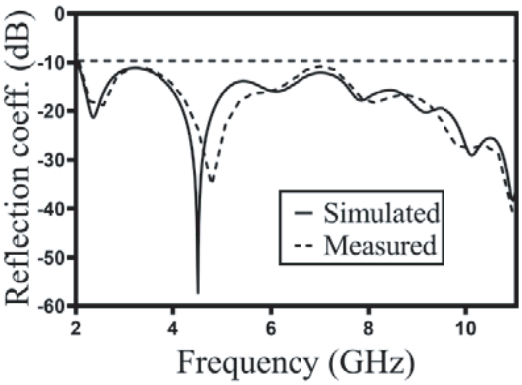

Figure 8. Comparison of simulated and measured reflection coefficients of the UWB monopole.

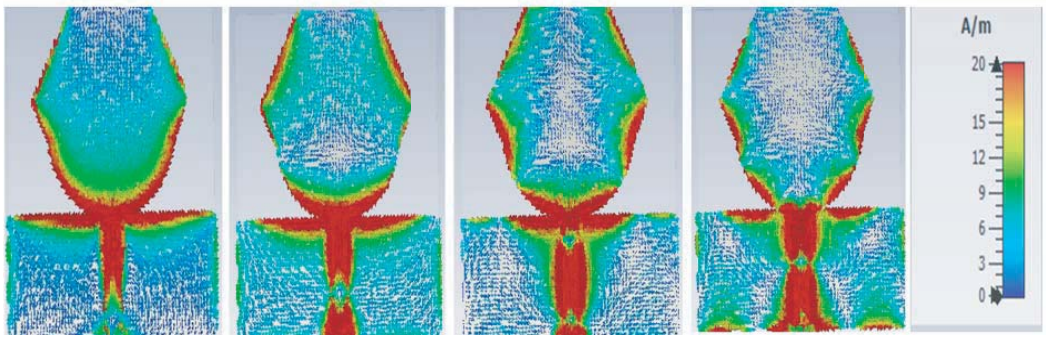

(a) (b) (c) (d)

Figure 9. Simulated surface current distribution of UWB sensing monopole in standalone configuration at (a) 2.352 GHz, (b) 4.513 GHz, (c) 8.1 GHz, and (d) 10.533 GHz.

good matching between simulation and experimental results. The small deviations are natural due to inherent measurement errors. In this figure, there are five distinct dips with two additional small dips. Understanding of this pattern needs observation of surface currents. Fig. 9 shows the surface current distributions at (a) 2.352 GHz, (b) 4.513 GHz, (c) 8.1 GHz, and (d) 10.533 GHz for the sensing antenna in a standalone configuration. These figures help in identifying areas on the ground plane with minimum current amplitudes. This is useful in locating places for narrowband antennas on the other side of the substrate for minimum coupling with the sensing antenna. On the ground plane, the surface current is mostly residing in the upper portion, i.e., the portion nearer to the radiator. Therefore, the antenna performance is independent of the ground plane length after a definite depth over which the surface current is appreciable. Further, Fig. 10 shows the surface current distributions on the sensing antenna for the integrated CR antenna system proposed in this work. These current distributions are at (a) 2.351 GHz, (b) 4.511 GHz, (c) 7.517 GHz, (d) 10.127 GHz, and (e) 10.838 GHz. At 2.351 GHz, the current extends from the feed-line to all sides, indicating the longest current path and hence the lowest operating frequency. However, the average current magnitude for this frequency is the lower than that for other frequencies. Therefore, the matching at this frequency is less than that for other frequencies, indicating the smallest dip in Fig. 8. At 4.511 GHz, the current on the arm L_1 is minimal, whereas the current distribution is strongly along the semi-circular portion and the arm L_2. Thus the effective current path for radiation is smaller than the previous case and hence a higher frequency. Due to the higher average power flow to the antenna, this frequency gives a sharp large dip in the reflection coefficient plot. But, higher-order modes start to appear at this frequency, which results in lower efficiency of the antenna although it accepts more power. In other words, this happens because radiated power in higher-order modes is less than that in the fundamental mode. At 7.517 GHz the

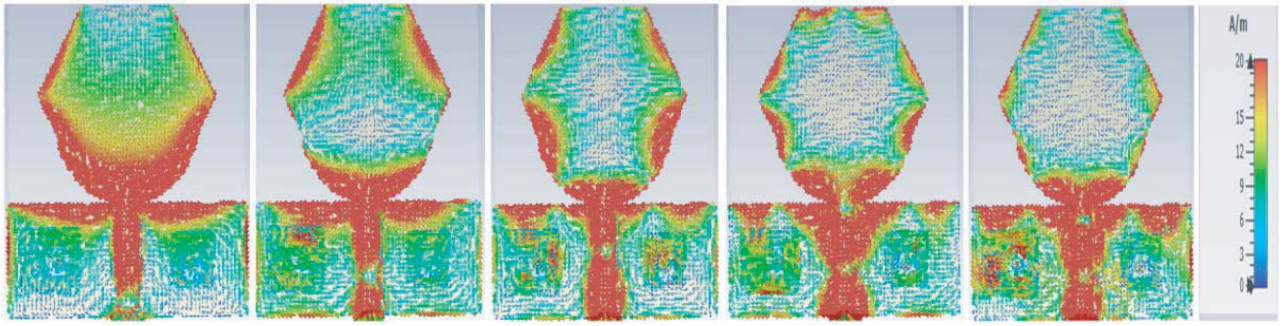

(a) (b) (c) (d) (e)

Figure 10. Simulated surface current distribution of integrated UWB sensing monopole antenna at (a) 2.351 GHz, (b) 4.511 GHz, (c) 7.517 GHz, (d) 10.127 GHz, and (e) 10.838 GHz.

formation of higher-order modes is clearly visible. The antenna receives more power than at 2.351 GHz but radiates less. More number of higher-order modes appears at 10.127 GHz resulting in the similar performance of the antenna. At 10.838 GHz, there are no more higher-order modes, but the current distribution is mostly prominent on the feed line, the ground plane around it, and the lower part of the antenna. At this frequency also the antenna receives high power but radiates comparatively less. In all these cases, the lower part of the antenna contains the major part of the input power and hence plays a dominating role in the radiations, thereby affecting the efficiency and radiation patterns. The remaining two peaks are spurious in nature and don't affect the antenna performance. The reason for this peak in the simulated curve may be due to the limitation in meshing imposed by the CST Microwave Studio on our license.

From the above discussions, it is clear that the sensing antenna has a good matching over the desired frequency band. Moreover, due to the dominating lower part, the radiation patterns are expected to be less distorted because of higher-order modes. Similarly, due to the absence of higher-order modes, the radiation efficiency is maximum at the lowest matching frequency and deteriorates marginally to 78% as higher-order modes appear with increasing frequencies (Fig. 12(b)). The simulated realized gains at respective frequencies are 2.08 dBi, 3.36 dBi, 5.32 dBi, and 5.5 dBi, which lie around a 2 dBi band indicating a nearly flat response of the antenna over the frequency band (Fig. 12(a)).

A sensing antenna in CR application requires a figure of eight (8) E-field patterns and omnidirectional H-field patterns. In other words, it is expected to resemble the pattern of a dipole. Fig. 11 shows the radiation patterns at (a) 2.351 GHz, (b) 4.511 GHz, (c) 7.517 GHz, and (d) 10.127 GHz for our proposed antenna. There is a close matching between simulated and measured results, except for some measurement errors. The first two frequencies clearly give the desired patterns. The patterns get distorted within an acceptable limit, as we move to higher frequencies because of the appearance of higher-order modes and to a less extent due to lossy FR-4 substrate at these frequencies.

3.2. NB Communicating Antennas

Figure 13 shows the current distribution on the U-slot loaded microstrip antenna. The slot acts as an inductor, and hence its loading pushes down the resonant frequency from that of an unloaded microstrip antenna. The current distribution shows that there is no disturbance compared to an unloaded microstrip antenna. Therefore, we expect its radiation characteristics to be similar to that of a rectangular microstrip antenna in its dominant mode. Its reflection coefficient (S_{22}) shows a sharp dip at 7.355 GHz (Fig. 14), confirming NB nature of the microstrip antenna to meet an NB antenna characteristic for a CR system. The radiation pattern (Fig. 15) conforms to that of a rectangular microstrip antenna without any distortion. The realized gain is 4.47 dBi, and the radiation efficiency is around 65% at 7.355 GHz, which is in the standard band for conventional rectangular microstrip antenna. This confirms that our design meets the requirement of an NB-CR antenna by using a miniaturized rectangular microstrip antenna with a U-slot for inductive loading. Close matching of simulated results for all characteristics, excluding current distribution, with measured value confirms the design process

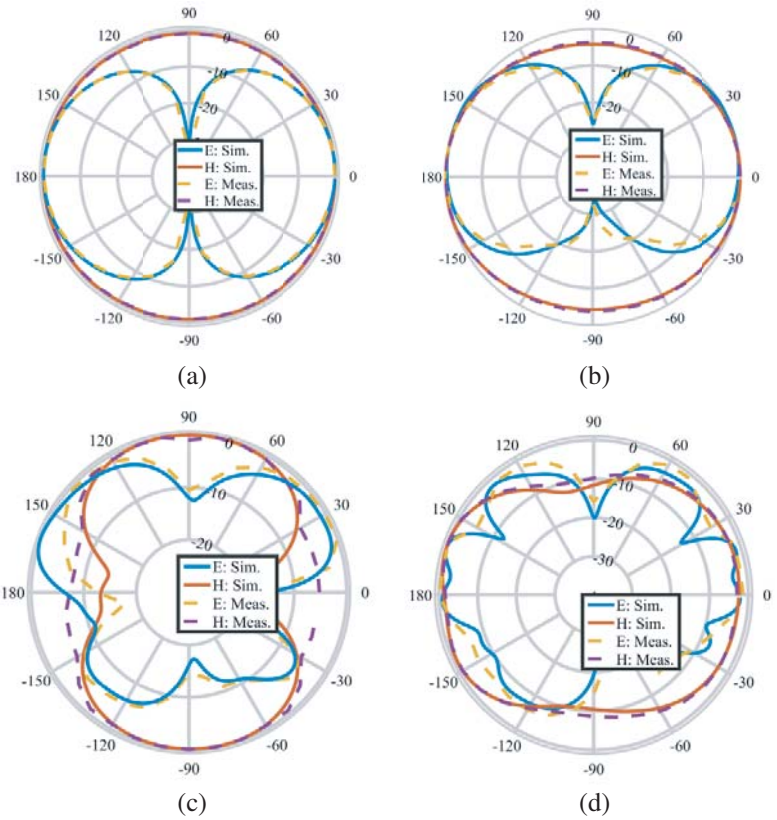

Figure 11. Simulated and measured radiation patterns of UWB sensing antenna at (a) 2.351 GHz, (b) 4.511 GHz, (c) 7.517 GHz, and (d) 10.127 GHz.

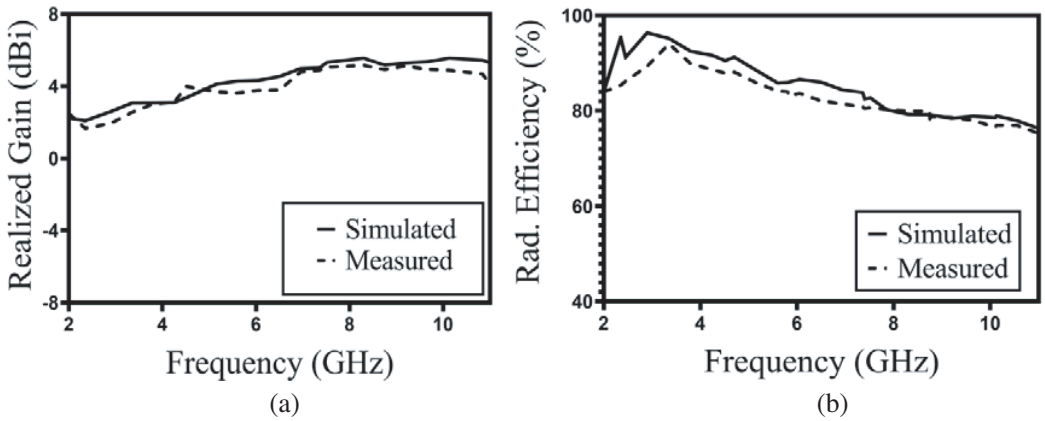

Figure 12. Comparison between simulated and measured results, (a) realized gain and (b) radiation efficiency of UWB antenna.

adopted for this NB antenna.

The reflection coefficient (S_{33}) plot of the G-shaped antenna in Fig. 16 confirms that the antenna operates in dual-band. The 1st resonating frequency is 5.834 GHz, and the 2nd is 8.786 GHz, confirming that they are not harmonically related. The surface current density plot in Fig. 17 verifies that there are no higher-order modes at the upper frequency. It shows that at 5.834 GHz, substantial current exists in the three parallel arms of the G structure. At this frequency, the current density is uniformly high on these arms, besides being moderately high on the sidearm. At 8.786 GHz, the current is moderately

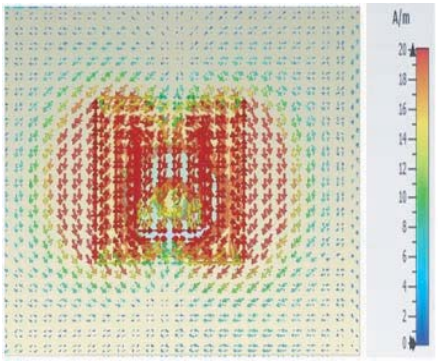

Figure 13. Simulated surface current distribution of U-slot NB antenna at 7.355 GHz.

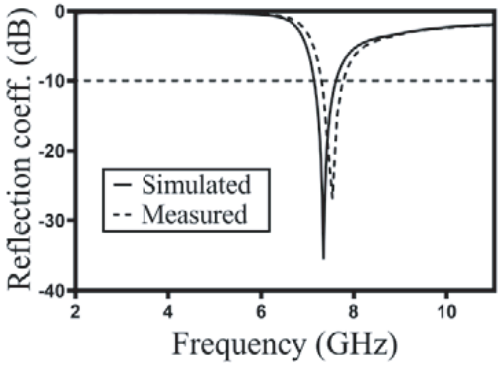

Figure 14. Comparison between simulated and measured reflection coefficients of U-slot NB antenna.

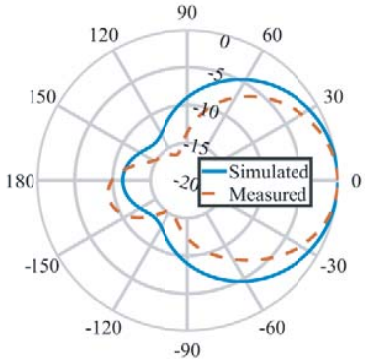

Figure 15. 2D radiation pattern of U-slot NB antenna at 7.355 GHz.

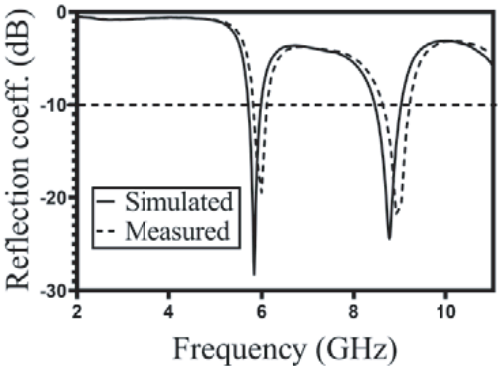

Figure 16. Comparison between simulated and measured reflection coefficients of G-shaped NB antenna.

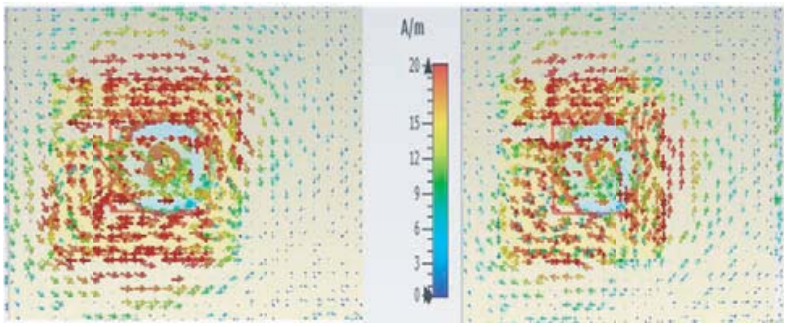

(a) (b)

Figure 17. Simulated surface current distribution of G-shaped NB antenna at (a) 5.834 GHz, and (b) 8.786 GHz.

distributed on all arms indicating a lower current density and a lower average current path than that for 5.834 GHz. Thus, it shows that the power delivered to the antenna from the source is marginally smaller at the upper frequency, indicating a slightly better matching at the lower frequency. A correlated interpretation of Fig. 17 with Fig. 16 confirms this, as the lower frequency dip is comparatively higher than that for the upper frequency. It shows (Fig. 22(a)) lower gains (2.76 dBi @ 5.834 GHz and 2.69 dBi @ 8.786 GHz) than U-slot loaded microstrip antenna but comparable efficiency of around 62% (Fig. 22(b)).

Its radiation patterns resemble that of a microstrip antenna (Fig. 18). At both frequencies, it maintains the pattern consistency. The design of the antenna is also being verified by comparing the closeness of the simulated and measured results, as in previous cases.

Figure 19 compares measured reflection coefficients (S_{44}) with those from simulations for four states ((a) ON-ON-ON, (b) OFF-OFF-OFF, (c) ON-ON-OFF, (d) OFF-OFF-ON) of the reconfigurable

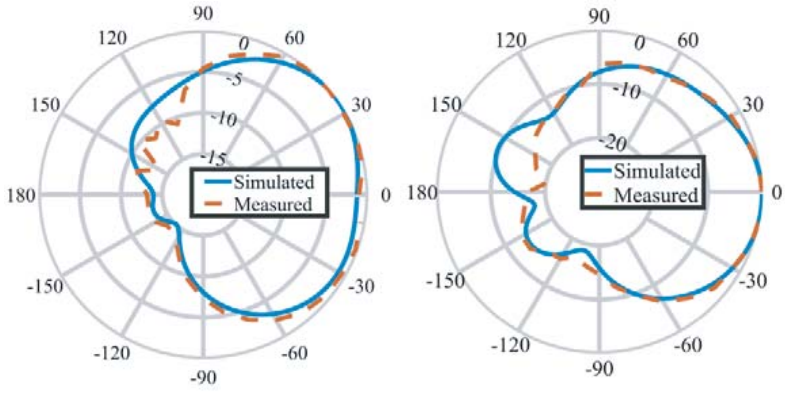

Figure 18. Simulated and measured 2D radiation patterns of G-shaped NB antenna at (a) 5.834 GHz, and (b) 8.786 GHz.

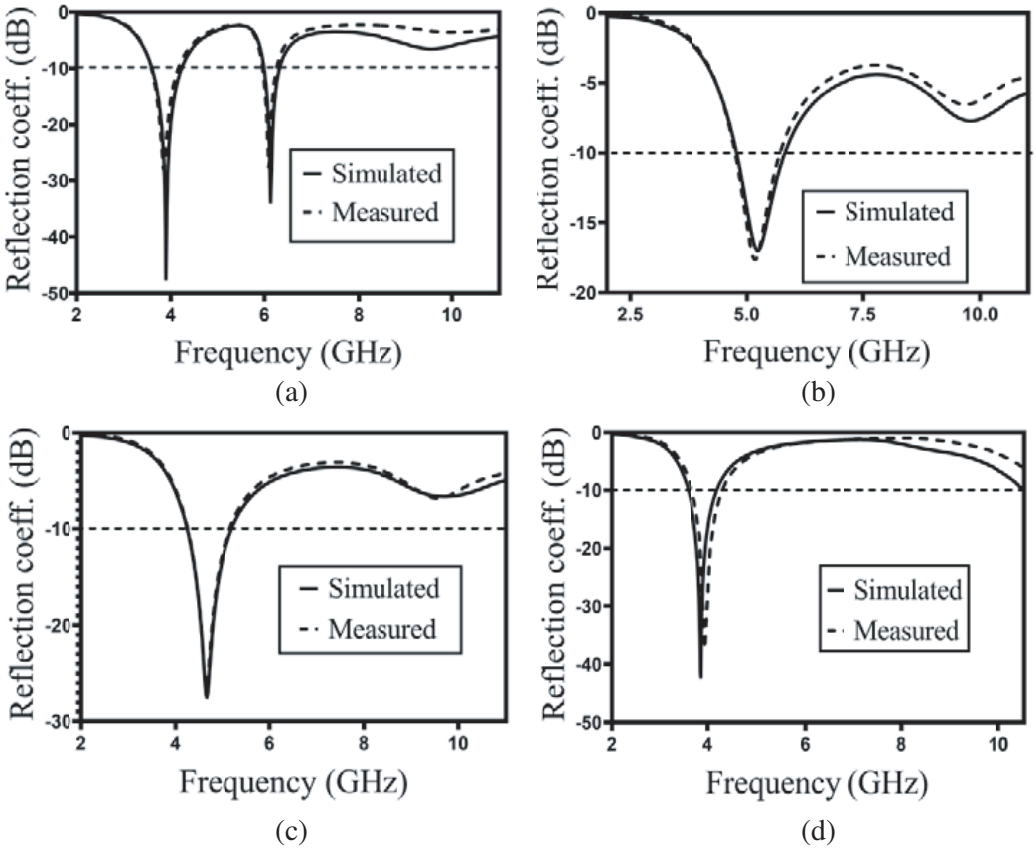

Figure 19. Simulated and measured reflection coefficient of the reconfigurable NB antenna, (a) ON-ON-ON state, (b) OFF-OFF-OFF state, (c) ON-ON-OFF state, and (d) OFF-OFF-ON state.

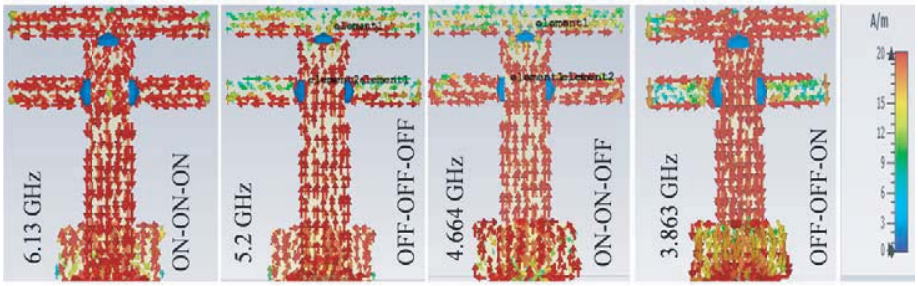

Figure 20. Simulated surface current distribution of the reconfigurable NB antenna, (a) ON-ON ON state, (b) OFF-OFF-OFF state, (c) ON-ON-OFF state, and (d) OFF-OFF-ON state.

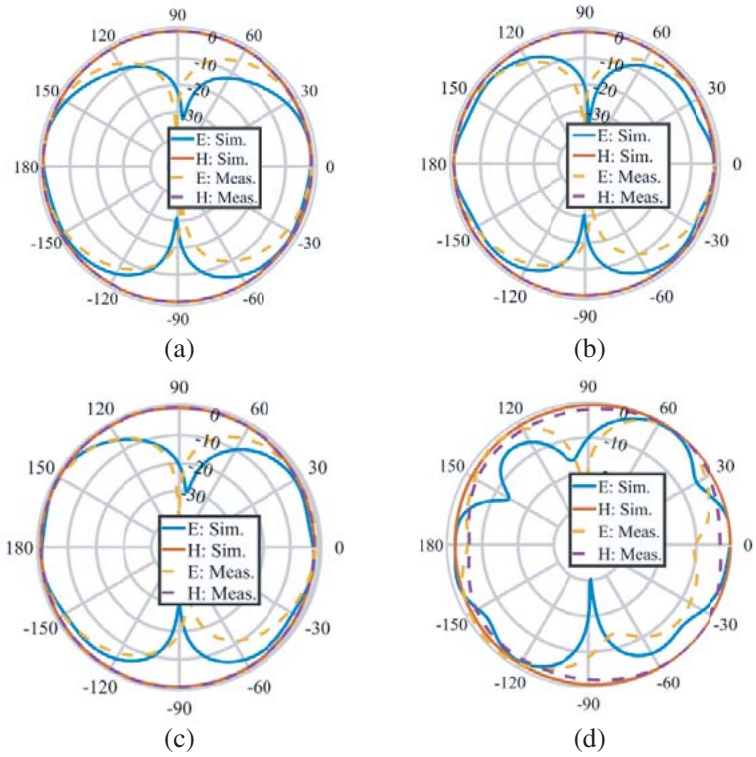

Figure 21. Simulated and measured E and H-plane radiation patterns of the reconfigurable antenna at (a) 3.863 GHz, (b) 4.664 GHz, (c) 5.2 GHz, and (d) 6.13 GHz.

antenna. There is only a minor mismatch validating the design process. Fig. 20 for current distributions in these states respectively, seen in conjunction with Fig. 19, gives insight into the functioning of this antenna. The main radiation comes from the central vertical patch, which is the stem of the antenna. In the state ON-ON-ON, this stem is loaded by two stubs on two sides and the conductor at its upper open-end. The currents on the lower two stubs are in opposite directions and hence do not contribute to radiation significantly. On the upper conductor, the current bifurcates at the entry point, and hence this is also an insignificant contributor to radiation. However, due to these loading effects, the main stem experiences two electrical lengths corresponding to two resonant frequencies of 3.863 GHz and 6.13 GHz. In the OFF-OFF-OFF state, the main stem experiences a current path corresponding to a resonant frequency at 5.2 GHz. In the ON-ON-OFF state, the loading on the main stem results in a current path of equivalent electrical length corresponding to the resonant frequency at 4.664 GHz. Similarly, the OFF-OFF-ON state gives an equivalent electrical length to the main stem for resonating

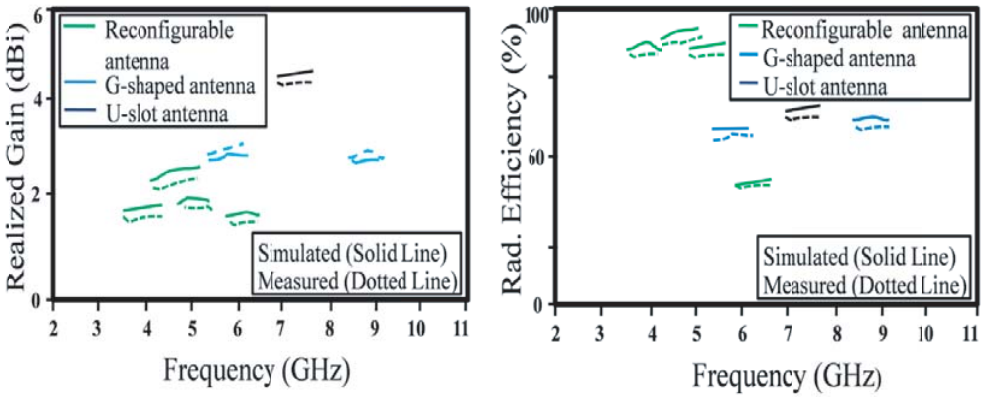

Figure 22. Simulated and measured (a) realized gain and, (b) radiation efficiency of all NB antennas.

at 3.863 GHz. It also indicates a high amount of out of phase current at 6.13 GHz, which can cause a significant reduction in radiation efficiency besides considerable distortion in the radiation pattern. A comparison of measured and simulated radiation patterns in Fig. 21 confirms this proposition for 6.13 GHz. In this figure, the patterns are almost consistent for the other three frequencies. The nature of the radiation patterns resembles the figure of eight (8), which is standard for CR communicating antennas. Table 3 summarizes the performance characteristics of these antennas. A point to note here is the fact that for convenience in the measurement, 1 Ω and 5 MΩ resistors were used to represent ON and OFF states of the p-i-n diode [40]. However, in practice, it is necessary to use p-i-n diodes with proper DC biasing circuits. For compatibility of measurement with simulation, we also used lumped resistors in simulation instead of p-i-n diodes. Fig. 22 shows the gain and efficiency of the reconfigurable antenna. The efficiency is above 80% for 3.863 GHz, 4.644 GHz, and 5.2 GHz, except for 6.13 GHz (around 50%).

Figure 23 shows the simulated isolation and Envelope Correlation Coefficient (ECC) curves of the CR antenna system. It reveals that the antenna system has below −15 dB mutual coupling throughout the UWB range (Fig. 23(a)). It is an acceptable value for minimum cross-talk between the antennas. We further calculated the ECC [42], using Eq. (8), which measures up to what extent the radiation patterns are uncorrelated. The ECC (max) values are presented in Table 2. It shows that the ECC (ρ) values between the ports lie below acceptable value 0.5 [17], over the entire operating band. That means the radiation patterns are not correlated. Table 4 compares the present CR antenna with earlier reported antennas in terms of physical dimension (substrate size) and band coverage. It shows that the proposed antenna has a smaller size and a larger coverage band.

$$\rho = \frac{\left|s_{ii}^{*}s_{ij} + s_{ji}^{*}s_{jj}\right|^{2}}{\left(1-\left|s_{ii}\right|^{2}-\left|s_{ji}\right|^{2}\right)\left(1-\left|s_{jj}\right|^{2}-\left|s_{ij}\right|^{2}\right)} \tag{8}$$

Table 2. Simulated ECC (max) of the proposed antenna system.

Between the antennas	ECC (max)
1 & 2	0.011
1 & 3	0.006
1 & 4	0.071
2 & 3	0.031
2 & 4	0.001
3 & 4	0.002

Table 3. Operational characteristics of CR antenna system.

Parameters	**G-shaped NB antenna**	**U-slot NB antenna**	**State-1 (S_1-ON, S_2-ON, S_3-ON)**	**State-2 (S_1-OFF, S_2-OFF, S_3-OFF)**	**State-3 (S_1-ON, S_2-ON, S_3-OFF)**	**State-4 (S_1-OFF, S_2-OFF, S_3-ON)**
Operating Frequencies (GHz)	5.834, 8.786	7.355	3.863, 6.13	5.2	4.664	3.863
Bandwidth (GHz)	5.70–6, 8.44–9.02	7.1–7.7	3.56–4.25, 5.96–6.36	4.76–5.70	4.21–5.21	3.56–4.25
Realized Gain (dBi)	2.76, 2.69	4.47	1.62, 1.22	2.2	1.92	1.64
Usable Band for application	LMI C-band, Maritime Radio Navigation	X-band	C-band	ISM, WLAN, Military application	Public safety	Next generation 5G (Mid-band)

Table 4. Comparison of various integrated CR antenna systems.

Ref.	**Substrate Size (mm^2)**	**Electrical size (λ_L^2)**	**UWB range (GHz)**	**Number of NB**	**Gain (UWB/ NB)**	**Efficiency (%) UWB/NB**	**Number of Ports**
[14]	68×54 ($= 3672$)	0.367	$3 \sim 11$	Four	$1.25 \sim 5$/ $0.6 \sim 4$	-/$37.2 \sim 75$	Two
[15]	80×65 ($= 5200$)	0.231	$2 \sim 5.5$	One	$3.92 \sim 7.2$/ 6.05	-/-	Two
[16]	58.35×75.7 (=4417)	0.534	$3.3 \sim 12$	Two	$0.5 \sim 6.5$/ $3 \sim 6$	-/-	Two
[17]	120×65 ($= 7800$)	0.038	$0.67 \sim 1.9$, $3 \sim 4.6$	Seven	$-5.26 \sim 3.12$/ $-0.96 \sim 4.90$	-/-	Five
[19]	63×63 ($= 3969$)	0.509	$3.4 \sim 8.0$	One	$2 \sim 6$/6	$47 \sim 60$/ $68 \sim 76$	Two
[20]	58×65.5 ($= 3799$)	0.459	$3.3 \sim 11$	Two	-/-	-/-	Two
[21]	120×65 ($= 7800$)	0.042	Communicating within UWB range from $0.7 \sim 3$	Five	-/$-4.45 \sim 0.23$	-/-	Four
Prop. Model	80×40 ($= 3200$)	0.142	$2.0 \sim 11$	Seven	$2.08 \sim 5.5$/ $1.2 \sim 4.47$	$78 \sim 85$/ $50 \sim 86$	Four

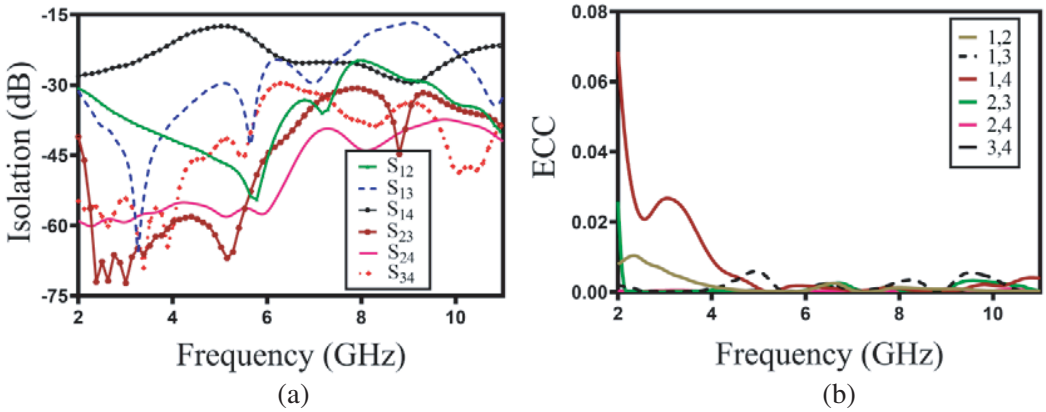

Figure 23. Simulated (a) isolation and (b) ECC plot of the CR antenna system.

4. CONCLUSION

This paper presented a compact, low profile multi-port CR antenna system. It proposed amalgamating a circle with pentagon to generate geometry for a planar monopole fed by a CPW so that its ground plane can be reused by NB communicating antennas. For the communication antennas, it proposed an NB U-slotted microstrip antenna and a G-shaped dual-band microstrip antenna besides a reconfigurable planar monopole antenna. The microstrip antennas were placed on opposite side of the UWB sensing antenna and used its ground plane with appropriate locations to minimize coupling. The reconfigurable antenna resided on the opposite end of the substrate. These NB antennas covered a total of seven sub-bands. The proposed antenna system meets the requirements of radiation characteristics for the CR system, like pattern, efficiency, gain, etc. With isolation less than −15 dB, the proposed antenna system is appropriate for C-band, ISM/WLAN/Military application, mid-band 5G, maritime radio navigation, X-band satellite communication, and public safety wireless communication.

ACKNOWLEDGMENT

The authors are thankful to the DST INSPIRE, Govt. of India, for providing financial support to R. K. PARIDA (IF160222) to pursue his doctoral program at Dept. of Electronic Science and Tech., Berhampur University.

REFERENCES

1. FCC, "FCC report and order on ultra wideband technology," Federal Commun. Commission, Washington, DC, USA, 2002.
2. Haykin, S., "Cognitive radio: Brain-empowered wireless communications," *IEEE Journal on Selected Areas in Communications*, Vol. 23, No. 2, 201–220, 2005.
3. Atapattu, S., C. Tellambura, and H. Jiang, *Energy Detection for Spectrum Sensing in Cognitive Radio*, 94, Springer Science & Business Media, 2014.
4. Tawk, Y., J. Costantine, and C. Christodoulou, *Antenna Design for Cognitive Radio*, 289, Artech House, 2016.
5. Zaidi, A., W. A. Awan, N. Hussain, and A. Baghdad, "A wide and tri-band flexible antennas with independently controllable notch bands for sub-6 GHz communication system," *Radioengineering*, Vol. 29, No. 1, 44–51, 2020.
6. Kumar, G. and R. Kumar, "A Survey on planar ultra-wideband antennas with band notch characteristics: principle, design, and applications," *AEU — International Journal of Electronics and Communications*, Vol. 109, 76–98, 2019.

7. Nella, A. and A. S. Gandhi, "A planar four-port integrated UWB and NB antenna system for CR in 3.1 GHz to 10.6 GHz," *IEEE National Conference on Communications*, 1–6, IEEE, Bangalore, India, 2019.
8. Hall, P. S., P. Gardner, and A. Faraone, "Antenna requirements for software defined and cognitive radios," *Proceedings of the IEEE*, Vol. 100, No. 7, 2262–2270, 2012.
9. Volakis, J., C. C. Chen, and K. Fujimoto, *Small Antennas: Miniaturization Techniques & Applications*, 448, McGraw Hill Professional, 2009.
10. Balani, W., M. Sarvagya, T. Ali, M. M. M. Pai, J. Anguera, A. Andujar, and S. Das, "Design techniques of super-wideband antenna — Existing and future prospective," *IEEE Access*, Vol. 7, 141241–57, 2019.
11. Ellis, M. S., Z. Zhao, J. Wu, Z. Nie, and Q. H. Liu, "Small planar monopole ultra-wideband antenna with reduced ground plane effect," *IET Microwaves Antennas Propagation*, Vol. 9, No. 10, 1028–34, 2015.
12. Chen, Z. N., T. S. P. See, and X. Qing, "Small printed ultrawideband antenna with reduced ground plane effect," *IEEE Transactions on Antennas and Propagation*, Vol. 55, No. 2, 383–88, 2007.
13. Midya, M., A. Chatterjee, and M. Mitra, "A printed CPW-fed ultra-wideband planar inverted-F antenna," *International Journal of Microwave and Optical Technology*, Vol. 15, 51–57, 2020.
14. Ebrahimi, E., J. R. Kelly, and P. S. Hall, "Integrated wide-narrowband antenna for multi-standard radio," *IEEE Transactions on Antennas and Propagation*, Vol. 59, No. 7, 2628–2635, 2011.
15. Nachouane, H., A. Najid, A. Tribak, and F. Riouch, "Dual port antenna combining sensing and communication tasks for cognitive radio," *International Journal of Electronics and Telecommunications*, Vol. 62, No. 2, 121–127, 2016.
16. Pahadsingh, S. and S. Sahu, "A two port UWB-dual narrowband antenna for cognitive radios," *Microwave and Optical Technology Letters*, Vol. 58, No. 8, 1973–78, 2016.
17. Jha, K. R., B. Bukhari, C. Singh, G. Mishra, and S. K. Sharma, "Compact planar multi-standard MIMO antenna for IoT applications," *IEEE Transactions on Antennas and Propagation*, Vol. 66, No. 7, 3327–3336, 2018.
18. Nella, A. and A. S. Gandhi, "A survey on planar antenna designs for cognitive radio applications," *Wireless Personal Communications*, Vol. 98, No. 1, 541–569, 2018.
19. Chacko, B. P., G. Augustin, and T. A. Denidni, "Electronically reconfigurable uniplanar antenna with polarization diversity for cognitive radio applications," *IEEE Antennas and Wireless Propagation Letters*, Vol. 14, 213–216, 2015.
20. Tawk, Y. and C. G. Christodoulou, "A new reconfigurable antenna design for cognitive radio," *IEEE Antennas and Wireless Propagation Letters*, Vol. 8, 1378–81, 2009.
21. Hussain, R. and M. S. Sharawi, "Planar four-element frequency agile MIMO antenna system with chassis mode reconfigurability," *Microwave and Optical Technology Letters*, Vol. 57, No. 8, 1933–1938, 2015.
22. Nella, A. and A. S. Gandhi, "Lumped equivalent models of narrowband antennas and isolation enhancement in a three antennas system," *Radioengineering*, Vol. 27, No. 3, 646–53, 2018.
23. Kumar, R. and R. Vijay, "Frequency agile quadrilateral patch and slot based optimal antenna design for cognitive radio system," *International Journal of RF and Microwave Computer-Aided Engineering*, Vol. 28, No. 2, 21176, 2018.
24. Kumar, R. and R. Vijay, "A frequency agile semicircular slot antenna for cognitive radio system," *International Journal of Microwave Science and Technology*, Vol. 2016, 1–11, 2016.
25. Kumar, R., P. Kumar, S. Singh, and R. Vijay, "Fast and accurate synthesis of frequency reconfigurable slot antenna using back propagation network," *AEU — International Journal of Electronics and Communications*, Vol. 112, 152962, 2019.
26. Mansoul, A., F. Ghanem, M. R. Hamid, and M. Trabelsi, "A selective frequency-reconfigurable antenna for cognitive radio applications," *IEEE Antennas and Wireless Propagation Letters*, Vol. 13, 515–518, 2014.

27. Kaur, R., D. Arora, R. Mittal, and R. Kumar, "Design and fabrication of compact frequency reconfigurable near-circular slot antenna for cognitive radio system applications," *Journal of Advanced Research in Dynamical and Control Systems*, Vol. 10, 2340–47, 2018.
28. Nella, A. and A. S. Gandhi, "A compact novel three-port integrated wide and narrow band antennas system for cognitive radio applications," *International Journal of Antennas and Propagation*, Vol. 2016, 1–14, 2016.
29. Sharma, S. and C. C. Tripathi, "An integrated frequency reconfigurable antenna for cognitive radio application," *Radioengineering*, Vol. 26, 746–754, 2017.
30. Nella, A. and A. S. Gandhi, "A five-port integrated UWB and narrowband antennas system design for CR applications," *IEEE Transactions on Antennas and Propagation*, Vol. 66, No. 4, 1669–76, 2018.
31. O, Y., Y. Jin, and J. Choi, "A compact four-port coplanar antenna based on an excitation switching reconfigurable mechanism for cognitive radio applications," *Applied Sciences*, Vol. 9, No. 15, 3157, 2019.
32. Liang, J., L. Guo, C. C. Chiau, X. Chen, and C. G. Parini, "Study of CPW-fed circular disc monopole antenna for ultra wideband applications," *IEE Proceedings — Microwaves Antennas and Propagation*, Vol. 152, No. 6, 520–526, 2005.
33. Ray, K. P. and S. S. Thakur, "Ultra wide band vertex truncated printed pentagon monopole antenna," *Microwave and Optical Technology Letters*, Vol. 56, No. 10, 2228–2234, 2014.
34. Ray, K. P., "Design aspects of printed monopole antennas for ultra-wide band applications," *International Journal of Antennas and Propagation*, Vol. 2008, 1–8, 2008.
35. Kundu, S., "Experimental study of a printed ultra-wideband modified circular monopole antenna," *Microwave and Optical Technology Letters*, Vol. 61, No. 5, 1388–1393, 2019.
36. Suh, S. Y., W. L. Stutzman, and W. A. Davis, "A new ultra-wideband printed monopole antenna: the planar inverted cone antenna (PICA)," *IEEE Transactions on Antennas and Propagation*, Vol. 52, No. 5, 1361–1364, 2004.
37. Martínez-Vázquez, M., M. Geissler, D. Heberling, A. Martínez-González, and D. Sánchez-Hernández, "Compact dual-band antenna for mobile handsets," *Microwave and Optical Technology Letters*, Vol. 32, No. 2, 87–88, 2002.
38. Deshmukh, A. A. and K. P. Ray, "Analysis and design of broadband U-slot cut rectangular microstrip antennas," *Sadhana*, Vol. 42, No. 10, 1671–1684, 2017.
39. Lee, K. F., S. L. Steven Yang, A. A. Kishk, and K. M. Luk, "The versatile U-slot patch antenna," *IEEE Antennas and Propagation Magazine*, Vol. 52, No. 1, 71–88, 2010.
40. Ullah, S., S. Ahmad, B. A. Khan, and J. A. Flint, "A multi-band switchable antenna for Wi-Fi, 3G advanced, WiMAX, and WLAN wireless applications," *International Journal of Microwave and Wireless Technologies*, Vol. 10, No. 8, 991–997, 2018.
41. Ullah, S., S. Hayat, A. Umar, U. Ali, F. A. Tahir, and J. A. Flint, "Design, fabrication and measurement of triple band frequency reconfigurable antennas for portable wireless communications," *AEU — International Journal of Electronics and Communications*, Vol. 81, 236–242, 2017.
42. Ren, J., W. Hu, Y. Yin, and R. Fan, "Compact printed MIMO antenna for UWB applications," *IEEE Antennas and Wireless Propagation Letters*, Vol. 13, 1517–20, 2014.